Molecular Plant • Volume 1 • Number 6 • Pages 990–1006 • November 2008 RESEARCH ARTICLE

Plasma Membrane-Associated SCAR Complex Subunits Promote Cortical F-Actin Accumulation and Normal Growth Characteristics in *Arabidopsis* Roots

Julia Dyachok[a,d], Mon-Ray Shao[a], Kevin Vaughn[b], Andrew Bowling[b], Michelle Facette[c], Stevan Djakovic[a,e], Lauren Clark[a] and Laurie Smith[a,1]

a Section of Cell and Developmental Biology, University of California San Diego, 9500 Gilman Drive, La Jolla, CA 92093-0116, USA
b Southern Weed Science Research Unit, USDA–ARS, 141 Experiment Station Road, Stoneville, MS 38776, USA
c Carnegie Institution, Department of Plant Biology, 260 Panama Street, Stanford, CA 94305, USA
d Present address: Division of Plant Biology, The Samuel Roberts Noble Foundation, 2510 Sam Noble Pkwy, Ardmore, OK 73401, USA
e Present address: Section of Neurobiology, University of California San Diego, 9500 Gilman Drive, La Jolla, CA 92093-0116, USA

ABSTRACT The ARP2/3 complex, a highly conserved nucleator of F-actin polymerization, and its activator, the SCAR complex, have been shown to play important roles in leaf epidermal cell morphogenesis in *Arabidopsis.* However, the intracellular site(s) and function(s) of SCAR and ARP2/3 complex-dependent actin polymerization in plant cells remain unclear. We demonstrate that putative SCAR complex subunits BRK1 and SCAR1 are localized to the plasma membrane at sites of cell growth and wall deposition in expanding cells of leaves and roots. BRK1 localization is SCAR-dependent, providing further evidence of an association between these proteins in vivo. Consistent with plasma membrane localization of SCAR complex subunits, cortical F-actin accumulation in root tip cells is reduced in *brk1* mutants. Moreover, mutations disrupting the SCAR or ARP2/3 complex reduce the growth rate of roots and their ability to penetrate semi-solid medium, suggesting reduced rigidity. Cell walls of mutant roots exhibit abnormal structure and composition at intercellular junctions where BRK1 and SCAR1 are enriched in the adjacent plasma membrane. Taken together, our results suggest that SCAR and ARP2/3 complex-dependent actin polymerization promotes processes at the plasma membrane that are important for normal growth and wall assembly.

Key words: cell expansion; cell morphogenesis; cytoskeleton; root biology; Arabidopsis.

INTRODUCTION

Plant cells acquire their shapes according to the patterns in which their walls expand during cell growth (Mathur, 2004). Actin filaments are thought to influence the expansion pattern of the cell wall by helping to direct the delivery of secreted wall material and membranes to sites of cell growth (Smith and Oppenheimer, 2005; Hussey et al., 2006). Numerous studies have established a role for the ARP2/3 complex in the spatial regulation of epidermal cell growth in plants (Szymanski, 2005). The animal Arp2/3 complex, consisting of seven subunits including the actin-related proteins Arp2 and Arp3, nucleates actin polymerization mainly by initiating new branches on the sides of existing actin filaments (Goley and Welch, 2006). Arp2/3 complex activity depends on nucleation promoting factors including members of the Scar/WAVE family (Stradal and Scita, 2005). In mammalian cells, Scar/WAVE is found in a complex with four other proteins: Sra1, Nap1, Abi1, and Hspc300 (Eden et al., 2002; Gautreau et al., 2004). In response to upstream regulators Rac and Nck, Scar/WAVE is activated via a mechanism that has been proposed to involve either dissociation of the complex or recruitment of the intact complex to sites of F-actin nucleation (reviewed, Takenawa and Suetsugu, 2007). Components of the Scar/WAVE complex localize to plasma membranes at the leading edge of animal cells where they nucleate cortical F-actin that promotes lamellipodial extension (Miki et al., 1998; Nozumi et al., 2003; Kunda et al., 2003; Rogers et al., 2003; Stovold et al., 2005).

Homologs of all mammalian Arp2/3 and Scar/WAVE complex subunits have been identified in *Arabidopsis*, including a family of four proteins distantly related to animal Scar/WAVE proteins (AtSCAR1 to AtSCAR4; Szymanski, 2005). Three of the

[1] To whom correspondence should be addressed. E-mail lgsmith@ucsd.edu, fax 858-534-7108, tel. 858-822-2531.

doi: 10.1093/mp/ssn059, Advance Access publication 8 October 2008
Received 17 June 2008; accepted 22 August 2008

four *Arabidopsis* SCAR proteins have been shown to stimulate mammalian Arp2/3 complex-dependent actin polymerization in vitro (Frank et al., 2004; Basu et al., 2005; Uhrig et al., 2007; Zhang et al., 2008). Although neither ARP2/3 nor SCAR complexes have been purified from plant extracts or reconstituted from plant subunits to date, numerous in-vitro and in-vivo binding interactions between putative complex subunits support the existence of ARP2/3 and SCAR complexes in plants (Szymanski, 2005; Uhrig et al., 2007). Mutations in genes encoding nine different subunits of the putative ARP2/3 or SCAR complexes dramatically perturb the growth patterns of epidermal hairs called trichomes and also reduce lobe outgrowth and intercellular adhesion in epidermal pavement cells (reviewed, Szymanski, 2005; Smith and Oppenheimer, 2005; also see more recent studies by Basu et al., 2005; Zhang et al., 2005; Djakovic et al., 2006; Le et al., 2006). Plants lacking all SCAR function are phenotypically equivalent to ARP2/3 complex subunit mutants (Zhang et al., 2008), and double mutants lacking both SCAR and ARP2/3 complex function are no more severe than either type of single mutant (e.g. El-Assal et al., 2004; Djakovic et al., 2006), suggesting that SCAR is the primary if not the sole activator of the ARP2/3 complex in *Arabidopsis*. Surprisingly, no severe loss of F-actin has been observed in ARP2/3 or SCAR complex subunit mutants. Instead, excessive bundling and spatial disorganization of cytoplasmic actin strands have been observed in expanding mutant trichomes, and alterations in cortical F-actin distribution have been observed in expanding mutant pavement cells (e.g. Mathur et al., 2003a; Le et al., 2003; Li et al., 2003; Deeks et al., 2004; Brembu et al., 2004; Djakovic et al., 2006).

In the moss *Physcomitrella patens*, ARP2/3 and SCAR complex subunit mutants have severe defects in filament elongation associated with loss or disruption of the F-actin 'cap' structure normally found at the apical growth site (Harries et al., 2005; Perroud and Quatrano, 2006, 2008; Finka et al., 2007). Moreover, ARPC4 (a subunit of the putative ARP2/3 complex) and BRK1 (the plant homolog of the Hspc300 subunit of the animal Scar/WAVE complex) are both specifically localized at the filament apex (Perroud and Quatrano, 2006, 2008). Thus, tip-localized activity of the SCAR–ARP2/3-dependent actin nucleation pathway plays a critical role in promotion of tip growth in *P. patens*. The ARP2/3 complex also promotes tip growth in elongating root hairs of *Arabidopsis*, but its role is minor and largely redundant with those of other actin regulatory proteins (Mathur et al., 2003b; Deeks et al., 2007). Although the genes encoding ARP2/3 and SCAR complex subunits are ubiquitously expressed (e.g. El-Assal et al., 2004; Basu et al., 2005; Uhrig et al., 2007), very little is known about roles for this pathway in vascular plants outside the context of expanding leaf epidermal cells and tip growing cells. Even in these cells, it remains unclear where SCAR and ARP2/3 complex-dependent actin nucleation occurs and what cellular processes are disrupted to cause the cell shape and adhesion defects observed in mutants.

Here, we use complementary methods to demonstrate that SCAR complex subunits are associated with the plasma membrane in various tissues of *Arabidopsis.* Analysis of roots of SCAR complex subunit mutants demonstrates an important role for SCAR and ARP2/3 complexes in accumulation of cortical (plasma membrane-associated) F-actin and in certain aspects of root growth and cell wall assembly. Together, these results provide new perspectives on the role(s) played by SCAR and ARP2/3 complex-dependent actin polymerization in plant cell growth.

RESULTS

BRK1 and SCAR1 Are Localized to the Cell Periphery

To gain insight into where SCAR- and ARP2/3-complex-dependent actin polymerization occurs in plant cells, we studied the localization of BRK1 and SCAR1 fluorescent fusion proteins in transgenic plants. BRK1::YFP expressed from the *BRK1* promoter is functional as indicated by its ability to complement the distorted trichome phenotype of *brk1* mutants (Figure 1C). In contrast to *scar2* mutants, which display a mild distorted trichome phenotype (Basu et al., 2005; Zhang et al., 2005), *scar1* mutants have normally shaped trichomes and lack any obvious phenotypes, although a redundant role for SCAR1 in trichomome morphogenesis is suggested by a slight enhancement of the *scar2* trichome phenotype in *scar1;scar2* double mutants (Zhang et al., 2008). Thus, to determine whether GFP::SCAR1 is functional in vivo, we tested its ability to rescue the *scar2* trichome phenotype when driven from the *SCAR2* promoter (since the wild-type *SCAR1* gene is not sufficient for normal trichome morphogenesis in *scar2* mutants, we reasoned that *SCAR1* promoter-driven expression of SCAR1::GFP would not rescue the *scar2* trichome phenotype). Indeed, normal trichome morphology was restored in *scar2* mutants transformed with *SCAR2p*::GFP::SCAR1 (Figure 1E). Thus, GFP::SCAR1 is functional because it can substitute for SCAR2 and we reasoned that the localization of *SCAR2p*::GFP::SCAR1 in complemented *scar2* mutants could provide information regarding the intracellular sites of SCAR1 and/or SCAR2 function.

Both BRK1::YFP and GFP::SCAR1 localized to the periphery of expanding trichomes (Figure 2A–2H). In young trichomes, BRK1::YFP and GFP::SCAR1 were enriched at the tips of newly initiated branches (Figure 2A–2D), presumably corresponding to sites of active cell growth. In partially expanded branches of older trichomes, BRK1::YFP and GFP::SCAR1 both remained peripherally localized but were spread along the full length of the elongating branch (Figure 2E–2H). At this stage, growth is also distributed along the entire length of the branch (Schwab et al., 2003). Thus, BRK1::YFP and GFP::SCAR1 appear to be localized at growth sites in expanding trichomes. GFP::SCAR1 was also associated with medium-sized intracellular organelles of unknown identity in expanding trichomes (Figure 2D). However, this component of the GFP::SCAR1 localization pattern was not observed for BRK1::YFP (Figure 2B).

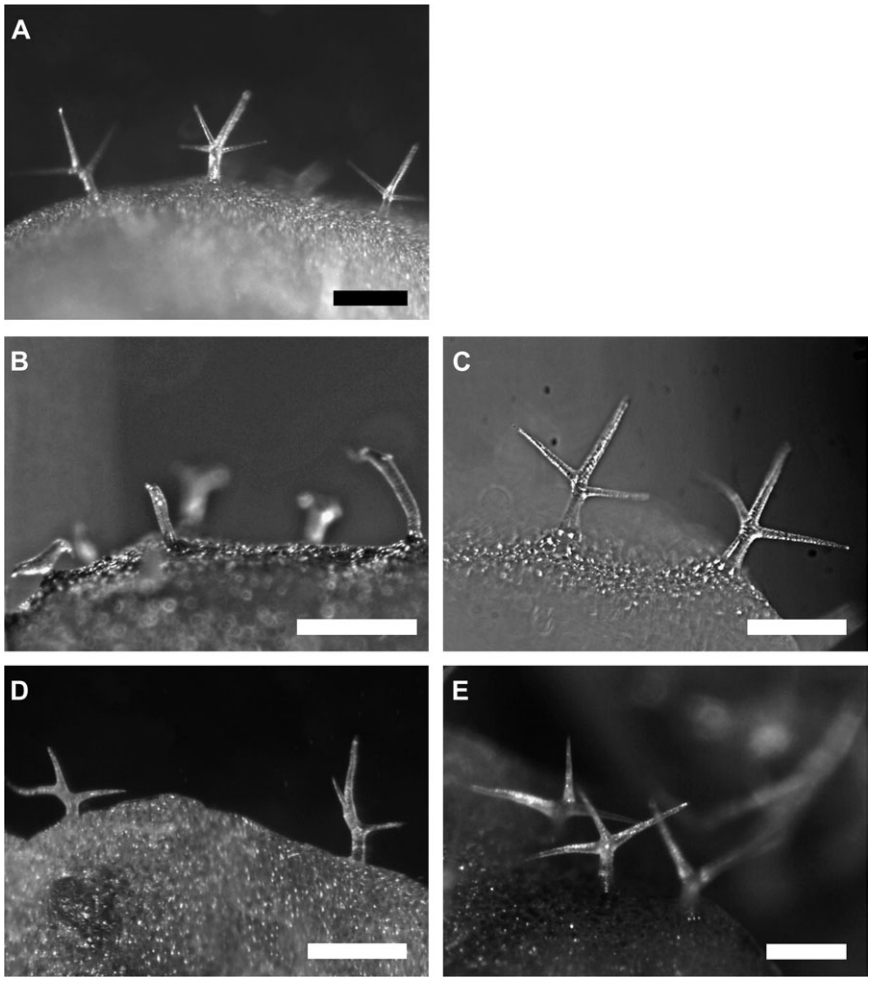

Figure 1. BRK1p::BRK1::YFP and SCAR2p::GFP::SCAR1 Restore Wild-Type Trichome Morphology in *brk1* and *itb1-16/scar2* Mutant Plants, Respectively.

Light micrographs of leaves.
(A) Columbia wild-type.
(B) *brk1* mutant (Columbia ecotype).
(C) *brk1* mutant expressing BRK1p::BRK1::YFP.
(D) *itb1-16 (scar2)* mutant (RLD ecotype).
(E) *itb1-16 (scar2)* mutant expressing SCAR2p::GFP::SCAR1.
Trichome morphology in RLD wild-type plants is indistinguishable from Columbia wild-type (Zhang et al., 2005) and is not shown. Scale bar = 250 microns.

Moreover, as described below, it was not observed for GFP::SCAR1 in other leaf epidermal cell types, or for endogenous SCAR1 detected by immunofluorescence in roots. Thus, the significance of organelle-associated SCAR1::GFP in trichomes is unknown, and may be artifactual.

BRK1::YFP and GFP::SCAR1 also localized to the cell periphery in expanding leaf epidermal pavement cells (Figure 2M–2P). Bright foci of higher fluorescence intensity were consistently observed at three-way intercellular junctions (henceforth referred to as 'cell corners') both in unexpanded pavement cells (arrows, Figure 2M and 2O) and in partially expanded ones that have already attained their characteristically lobed shapes (arrows, Figure 2N and 2P). These foci of BRK1::YFP and GFP::SCAR1 presumably correspond to sites of increased deposition of cell wall material, which fills the triangular-shaped spaces found at three-way wall junctions. Partially expanded pavement cells also exhibited more diffusely localized enrichments of BRK1::YFP and GFP::SCAR1 at points of maximum curvature (arrowheads, Figure 2N and 2P), which might correspond to sites of lobe outgrowth.

We next examined the localization of BRK1 and SCAR1 proteins in root tips. While no clear BRK1::YFP localization could be detected in epidermal cells including elongating root hairs (data not shown), cortical and endodermal cells of the root tip showed peripherally localized BRK1::YFP predominantly at transverse cell ends, which was markedly enriched at cell corners as observed in leaves (arrows, Figure 2Q) and persisted as these cells elongated (Figure 2R). SCAR1 localization in roots was investigated via whole mount immunofluorescent labeling with a previously characterized anti-SCAR1 antibody (Djakovic et al., 2006). Similar to localization results for BRK1::YFP, anti-SCAR1 staining was observed at the periphery of cells in internal layers of the root, and was often concentrated at cell corners (arrows, Figure 2T). This labeling could be attributed to SCAR1 because it was absent in *scar1* mutants (Figure 2S), which were previously shown to lack SCAR1 protein via Western blot analysis (Djakovic et al., 2006). Nonspecific cytoplasmic staining by the anti-SCAR1 antibody obscures detection of SCAR1 in root and leaf epidermal cells, including trichomes (data not shown). In summary, BRK1::YFP, GFP::SCAR1, and endogenous SCAR1 showed very similar patterns of localization at the cell periphery in both leaves and roots.

Consistent with previous analyses demonstrating ubiquitous expression of *BRK1* (Djakovic et al., 2006; Le et al.,

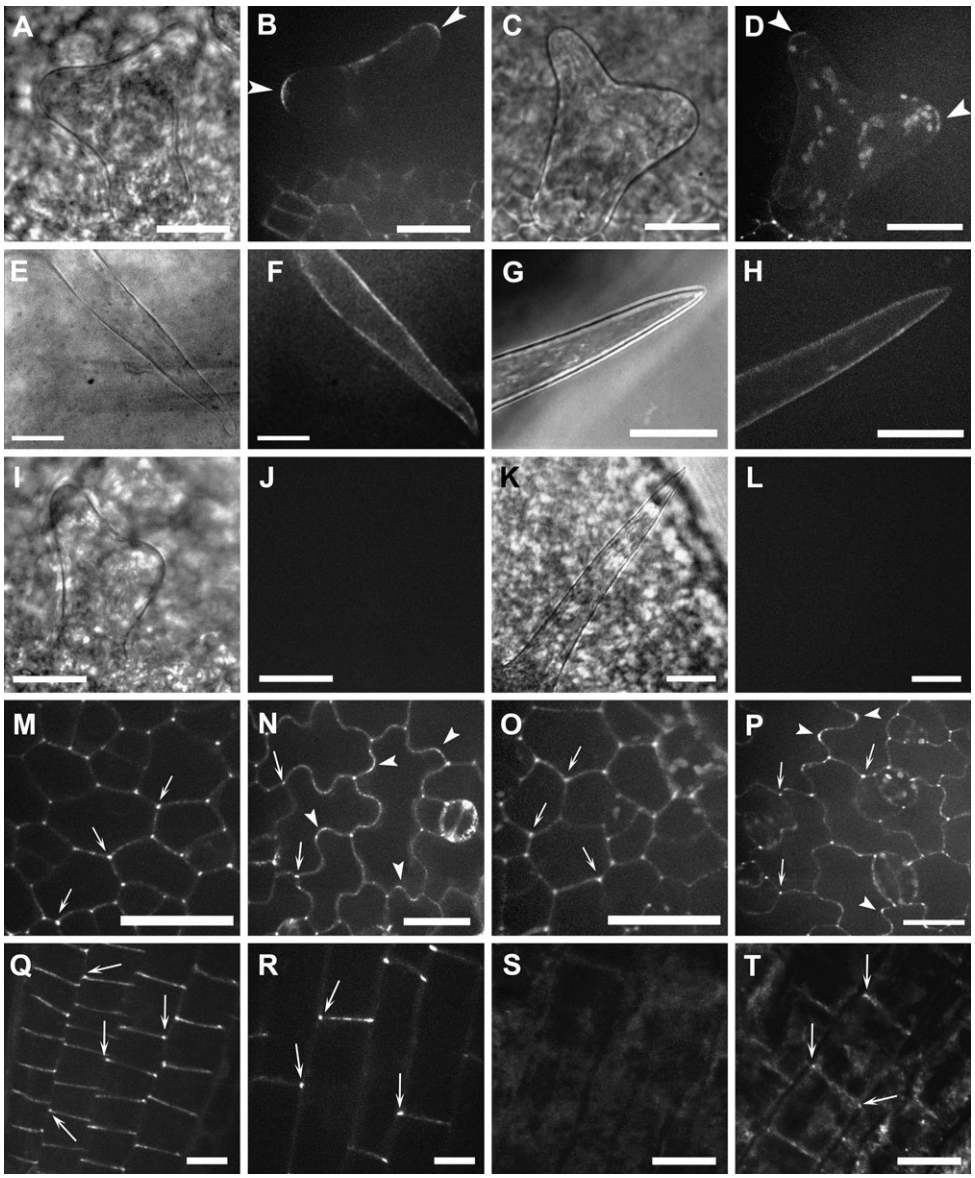

Figure 2. BRK1::YFP, GFP::SCAR1 and SCAR1 Localize to the Cell Periphery.

(A–L) Trichomes at early (A–D, I, J) and later (E–H, K, L) stages of expansion. Brightfield (A, E) and confocal fluorescence (B, F) images of complemented *brk1* mutants expressing *BRK1p*::BRK1::YFP. Brightfield (C, G) and confocal fluorescence (D, H) images of wild-type plants expressing *SCAR2p*::GFP::SCAR1. Arrowheads in (B) and (D) point to local enrichments of fluorescence seen at tips of newly emerged trichome branches. Brightfield (I, K) and confocal fluorescence (J, L) images of non-transgenic trichomes acquired under the same conditions (laser power, exposure time, etc.) employed for transgenic trichomes showed no detectable fluorescence, confirming that the fluorescence shown in (B, D, F, H) is due to the presence of YFP/GFP and not to autofluorescence.

(M–P) Leaf epidermal pavement cells that are unexpanded (M, O) or partially expanded (N, P). (M, N) Complemented *brk1* mutants expressing *BRK1p*::BRK1::YFP. (O, P) Complemented *itb1-16/scar2* mutants expressing *SCAR2p*::GFP::SCAR1. Arrows in (M–P) point to cell corners showing local enrichments of fluorescence. Arrowheads in (N) and (P) point to broader, localized enrichments observed at points of maximum curvature in partially expanded pavement cells.

(Q–T) BRK1::YFP and SCAR1 localization in root cortical cells. (Q, R) Complemented *brk1* mutant expressing *BRK1p*::BRK1::YFP. (S, T) Confocal fluorescence images of *scar1* mutant (S, negative control) and wild-type (T) roots fixed and stained with anti-SCAR1 antibody. Arrows in (Q, R, T) point to cell corners showing local enrichments of fluorescence. Scale bar = 20 microns in (A–P); 10 microns in (Q–T).

2006), we found that *BRK1p*::BRK1::YFP was present in a wide variety of cell types surveyed in addition to those described above, including expanding epidermal cells of hypocotyls, cotyledons, gynoecia, anther filaments, petals, and sepals, as well as fully expanded leaf epidermal pavement and guard cells. Peripheral localization of BRK1::YFP was observed in all of these cell types with foci at cell corners as described for expanding leaf and root cells (data not shown). These

observations suggest that BRK1's function in expanding cells is not restricted to those exhibiting shape abnormalities in *brk1* mutants, and that it has a role to play even in cells that are no longer growing.

BRK1 and SCAR1 Are Peripherally Associated with Plasma Membrane

The plasma membrane is attached to the cell wall, and differentiating plasma membrane versus cell wall localization is difficult at the light microscope level. To determine whether BRK1::YFP is associated with the plasma membrane or cell wall, we analyzed its localization in root cells after retraction of the plasma membrane from the cell wall via plasmolysis with sucrose. In plasmolyzed cells, BRK1::YFP (including the foci of BRK1::YFP found at cell corners) retracted from the cell wall with the plasma membrane, indicating its association with the plasma membrane rather than the cell wall (Figure 3).

We further used a biochemical approach to determine whether BRK1::YFP and/or SCAR1 are membrane-associated. In Western blots of unfractionated seedling extracts, BRK1::YFP and SCAR1 were barely detectable using anti-GFP and anti-SCAR1 antibodies, respectively (data not shown). Consistent with a membrane association for both proteins, when extracts were separated into microsomal and soluble fractions by ultracentrifugation, the majority of SCAR1 and BRK1::YFP were found in the microsomal fraction with the membrane marker protein α-1,2-Mannosidase I (Preuss et al., 2004), whereas the cytoplasmic marker protein PUX1 (Rancour et al., 2004) was mostly found in the soluble fraction (Figure 4). To investigate the nature of their association with the microsomal fraction, we attempted to extract BRK1::YFP and SCAR1 from microsomal pellets under various conditions. Both BRK1::YFP and SCAR1 were partially solubilized with detergents or 0.1 M Na_2CO_3 but not with 2 M NaCl, suggesting a peripheral membrane association (Figure 5). Consistent with these findings and with the lack of a signal peptide or transmembrane domain in BRK1, BRK1::YFP failed to accumulate intracellularly upon treatment with brefeldin A, a secretion inhibitor, suggesting that BRK1::YFP is targeted to the plasma membrane via a secretion-independent pathway (Figure 6).

SCARs Are Required for Plasma Membrane Localization of BRK1::YFP

Arabidopsis SCARs bind to BRK1 in vitro (Frank et al., 2004; Zhang et al., 2005), suggesting a possible role for one of the proteins in localization of the other. To investigate this possibility, we analyzed the localization of transiently expressed BRK1::YFP following bombardment into expanding epidermal pavement cells of wild-type plants and mutants lacking SCAR function. To avoid any possible ambiguity arising from functional redundancy among members of the SCAR family (Zhang et al., 2008), we constructed a *scar1,2,3,4* quadruple mutant for this experiment (see Methods for details). For comparison with *scar* quadruple mutants, we also analyzed BRK1::YFP localization in *arp2* mutants. However, we could not investigate the dependence of SCAR1 localization on BRK1, because SCAR proteins are degraded in the absence of BRK1 (Djakovic et al., 2006; Le et al., 2006).

For unknown reasons, transiently expressed BRK1::YFP showed more cytoplasmic localization than was observed in stable BRK1::YFP transgenics, even when expressed at very low levels. In highly vacuolated cells such as epidermal pavement cells, plasma membrane-associated fluorescence is not readily discernable in the presence of cytoplasmic fluorescence, which is concentrated at the cell periphery in a thin layer of cortical cytoplasm. However, we observed that at junctions between wild-type pavement cells and guard cells, transiently expressed BRK1::YFP typically showed localized accumulation at cell corners (arrow, Figure 7A)—a characteristic feature of BRK1::YFP localization in stable BRK1::YFP transgenic plants that was clearly distinguishable from cytoplasmic BRK1::YFP. Quantitative analysis showed that in wild-type pavement cells, bright foci of BRK1::YFP were present at 75% of corners associated with junctions between pavement

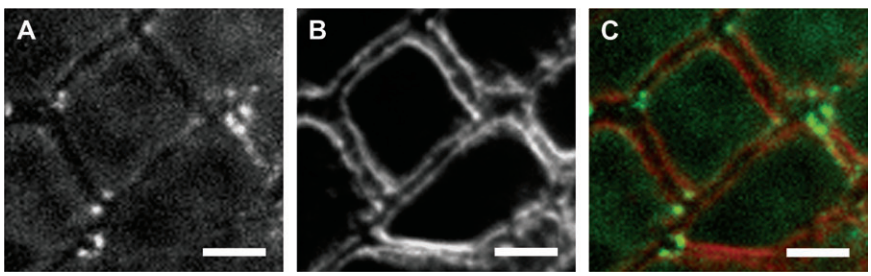

Figure 3. BRK1::YFP and SCAR1 Remain Associated with Plasma Membranes after Plasmolysis.

Confocal fluorescence images of root tip cells of complemented *brk1* mutants illustrating BRK1p::BRK1::YFP fluorescence immediately after partial plasmolysis with 0.5 M sucrose (monochrome in **(A)**, green in **(C)**) in relation to plasma membranes labeled with FM4-64 (monochrome in **(B)**, red in **(C)**). Cells were only partially plasmolysed for these experiments because, for unknown reasons, plasmolysis caused loss of BRK1::YFP from the cell periphery. Even with only partial plasmolysis, some BRK1::YFP was lost from the cell periphery, causing the BRK1::YFP signal to appear fainter and more restricted to cell corners than it does in Figure 2Q. Scale bar = 10 microns.

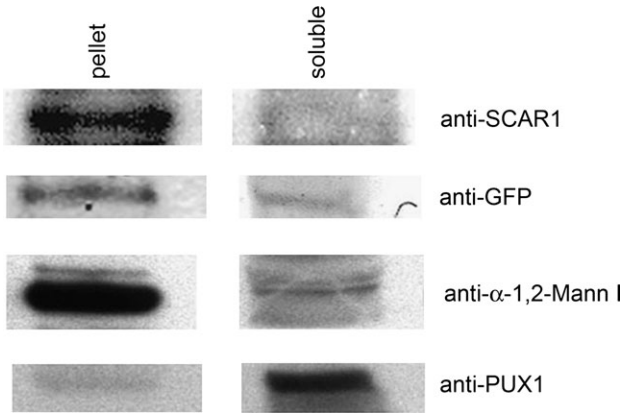

Figure 4. BRK1::YFP and SCAR1 Are Enriched in the Microsomal Fraction of Plant Tissue Extracts.

Extracts were ultra-centrifuged to separate microsomal membranes ('pellet') from supernatants ('soluble'). Western blots were probed with the indicated antibodies (see Methods for details regarding procedures and antibodies). The bands shown are consistent with the predicted molecular masses of SCAR1 and BRK1::YFP and confirmed as SCAR1 and BRK1::YFP by their absence in samples derived from *scar1* mutants and non-transgenic plants, respectively, which were processed in parallel but are not shown in the figure.

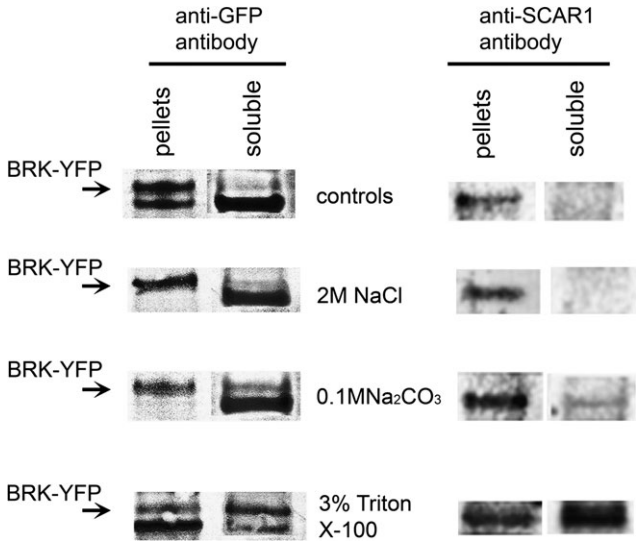

Figure 5. BRK1::YFP and SCAR1 Behave Biochemically as Peripheral Membrane Proteins.

Microsomal membrane pellets were re-suspended in the original extraction buffer alone ('controls') or with this buffer supplemented with the indicated reagents, and subsequently ultra-centrifuged to separate solubilized proteins ('soluble') from those remaining insoluble ('pellets'). Western blots of each sample were probed with anti-GFP to detect BRK1::YFP (arrows, left panel) or with anti-SCAR1 (right panel). BRK1::YFP and SCAR1 remain insoluble in the buffer alone (control) and 2 M NaCl samples, but are partially extracted from the microsomal pellet with 0.1 M Na_2CO_3 and 3% Triton X-100. Bands identified as BRK1::YFP and SCAR1 are consistent with their predicted molecular masses and their identities were confirmed by their absence from samples derived from non-transgenic plants and *scar1* mutants, respectively, which were processed in parallel but are not shown in the figure.

and guard cells (n = 24). The proportion of such corners showing bright foci of BRK1::YFP was not significantly different in *arp2* mutants (76.5%, n = 34; Figure 7B), but was reduced in *scar1,2,3,4* quadruple mutants to 11.5% (n = 26, significantly different from wild-type at $p < 0.0001$ by Fisher's Exact Test; Figure 7C). Thus, localization of BRK1 at cell corners depends on SCAR but not the ARP2/3 complex.

Cortical Actin Is Partially Depleted in Root Tip Cells of *brk1* Mutants

The Scar/WAVE complex is localized to sites of actin nucleation in animal cells, and its depletion markedly abolishes actin polymerization at those sites (Miki et al., 1998; Rogers et al., 2003; Kunda et al., 2003; Innocenti et al., 2004). Localization of BRK1::YFP and GFP::SCAR1 at the plasma membrane suggests a role for the SCAR complex in promotion of cortical F-actin polymerization. Previous studies have not reported depletion of cortical F-actin in expanding trichomes or pavement cells of SCAR or ARP2/3 complex subunit mutants (Li et al., 2003; Djakovic et al., 2006), but actin has not been previously examined in roots of these mutants. Therefore, we examined F-actin in root tips of *brk1* mutants, focusing on internal tissue layers where plasma membrane localization of BRK1::YFP and SCAR1 was observed.

We visualized F-actin in plants expressing an actin binding domain of fimbrin tagged at both ends with GFP (GFP::ABD2::GFP) (Wang et al., 2008). As illustrated in Figure 8A, GFP::ABD2::GFP revealed cortical F-actin mainly at the transverse ends of wild-type root cells. Interestingly, cortical F-actin was often enriched at cell corners (arrowheads, Figure 8A and 8C) where BRK1::YFP and SCAR1 are also enriched. Cortical F-actin visualized by this method was markedly depleted in *brk1* mutant root tips (Figure 8B and 8D). We also visualized F-actin via whole-mount immunolabeling of fixed root tips. This approach also revealed cortical F-actin at the transverse ends of most wild-type root tip cells, which often appeared enriched at cell corners (Figure 8G), and depletion of cortical F-actin at transverse cell ends and cell corners in *brk1* mutants (Figure 8H).

To further analyze the difference between wild-type and *brk1* mutant, F-actin density was analyzed quantitatively at cell corners in GFP::ABD2::GFP transgenic plants where differences between wild-type and *brk1* appeared most pronounced. Computer-generated cross-sections were made through Z-stack projections at cell corners (examples of section planes are illustrated with dashed lines in Figure 8A and 8B) and displayed in the X/Y plane as shown in Figure 8E and 8F. For each corner analyzed, we calculated the ratio of fluorescence intensity at the intercellular junction (arrowheads, Figures 8E and 8F) relative to background (sampled in the adjacent vacuole as indicated by circles in Figure 8E and 8F). The average ratio in *brk1* mutants (1.47 ± 0.15, n = 135 junctions total from 15 roots) was significantly lower than that in

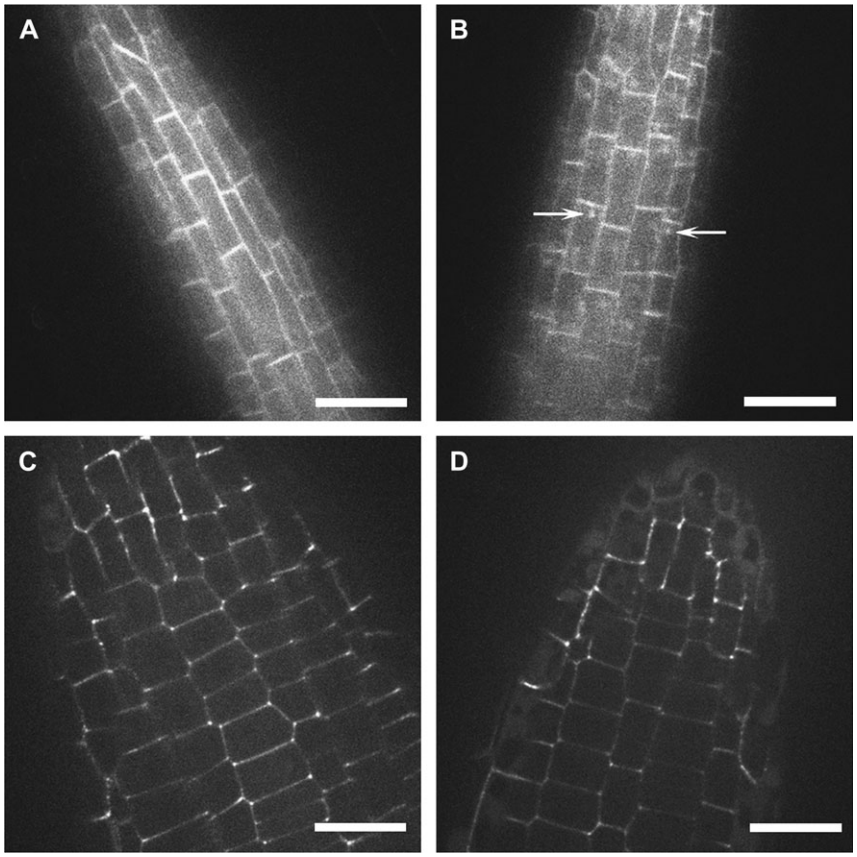

Figure 6. BRK1::YFP Localization in Root Cells Is Not Altered by Treatment with Brefeldin A (BFA) for 30 min.

As previously described (Geldner et al., 2001), PIN1::GFP is localized at the plasma membrane of root tip cells **(A)** but treatment with 50 mM BFA for 30 min caused partial loss of PIN1::GFP from the plasma membrane and its accumulation in BFA bodies (Royle and Murrell-Lagnado, 2003) (arrows, **(B)**). BRK1::YFP is localized at the cell periphery both before **(C)** and after 30 min of treatment with 50 mM BFA **(D)**. Scale bar = 20 microns.

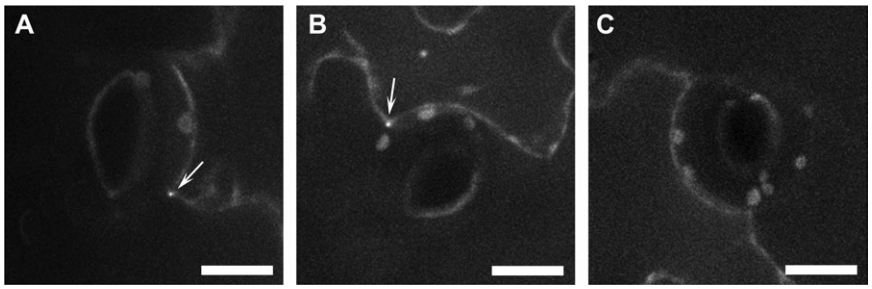

Figure 7. SCAR-Dependent Localization of BRK1p::BRK1::YFP Transiently Expressed in Expanding Cotyledon Pavement Cells.

(A) Wild-type, **(B)** *arp2* mutant, and **(C)** *scar 1,2,3,4* quadruple mutant. Arrows in (A) and (B) indicate bright foci of BRK1::YFP found at cell corners associated with junctions between epidermal pavement and guard cells in wild-type and *arp2* mutant leaves, but not in *scar 1,2,3,4* quadruple mutant leaves. Peripheral YFP fluorescence outlining transformed pavement cells in all three panels is attributable to the cytoplasm based on the presence of fluorescent transvacuolar cytoplasmic strands in focal planes not shown here. Scale bar = 10 microns.

wild-type (2.36 $\pm$ 0.4, n = 175 junctions total from 19 roots) ($p < 0.00001$ by student's t-test).

SCAR and ARP2/3 Complex Subunit Mutants Have Altered Root Growth Characteristics

Our findings that SCAR complex subunits are plasma membrane-localized in root cells and that the SCAR complex is required for normal cortical F-actin accumulation in these cells raised the question of what actin-dependent processes might be disrupted in roots of SCAR and ARP2/3 complex subunit mutants, which has not been previously addressed. Several aspects of root growth are known to be actin-dependent, including gravitropism and elongation rate (Blancaflor et al., 2006). We found that root gravitropic responses were not significantly altered in ARP2/3 and SCAR complex subunit mutants (data not shown). However, root growth rates were significantly reduced in all mutants examined (Figure 9A). Moreover, we observed that roots of all mutants were deficient in their ability to penetrate semi-solid medium. This deficiency did not appear to be due to the reduced growth rate of mutant roots, since both wild-type and mutant roots efficiently penetrated media containing 0.5% agar, but increasing

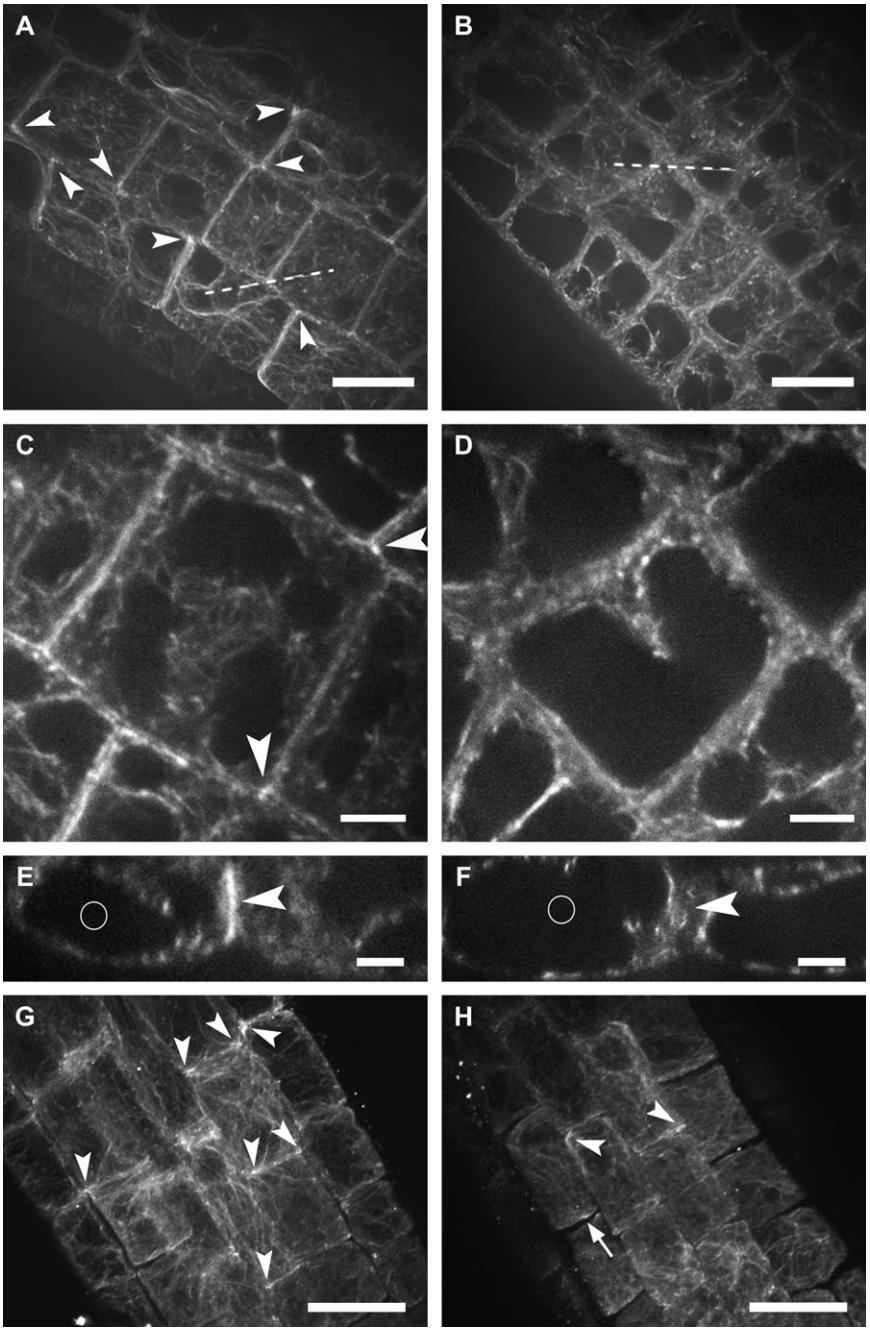

Figure 8. Cortical F-actin Is Depleted in Internal Tissue Layers of *brk1* Mutant Root Tips.

(A–F) Actin visualized by expression of GFP::ABD2::GFP in living cells of wild-type (A, C, E), and *brk1* mutant (B, D, F). (A) and (B) are Z-stack projections; (C) and (D) are single focal planes shown at higher magnification. Arrowheads in (A) and (C) point to local accumulations of cortical F-actin observed at cell corners in wild-type. (E) and (F) are computer-generated cross-sections made through Z-stack projections in the planes indicated by dashed lines in (A) and (B) (arrowheads and circles illustrate junction and background areas, respectively, sampled for quantitative analysis of F-actin density).

(G, H) Actin visualized by whole mount immunofluorescence of fixed wild-type (G) and *brk1* (H) root tips. Z-stack projections are shown. Arrowheads point to local accumulations of cortical F-actin seen frequently at cell corners in wild-type and less often in *brk1* mutants; arrow in (H) illustrates an example of discontinuous cortical F-actin at a transverse cell end in a *brk1* root tip. Scale bar = 20 microns in (A, B, G, H); 5 microns in (C, D); 2.5 microns in (E, F).

the agar concentration to 1.25% impaired the penetration of mutant roots significantly more than wild-type roots (Figure 9B). Expression of BRK1::YFP in *brk1* mutants restored the wild-type efficiency of agar penetration (Figure 9B), confirming that the agar penetration deficiency observed in *brk1* mutants is due to loss of BRK1.

Cell Wall Ultrastructure Is Altered at Three-Way Cell Junctions in Mutant Roots

The reduced ability to penetrate semi-solid medium observed for SCAR and ARP2/3 complex mutant roots might be due to alterations in cell wall structure or composition resulting in loss of rigidity in root cell walls. To investigate possible wall alterations in mutant roots, we began with biochemical analyses of wall composition. Gas chromatography analyses indicated similar amounts of neutral monosaccharides in cell walls isolated from wild-type, *brk1*, and *arp2* roots (Table 1). Electron microscopy revealed normal cell wall ultrastructure in most areas of *brk1* and *arp2* mutant root tips. However, at the transition between division and elongation zones where cells are beginning to elongate, ultrastructural abnormalities were occasionally observed at three-way intercellular junctions. A

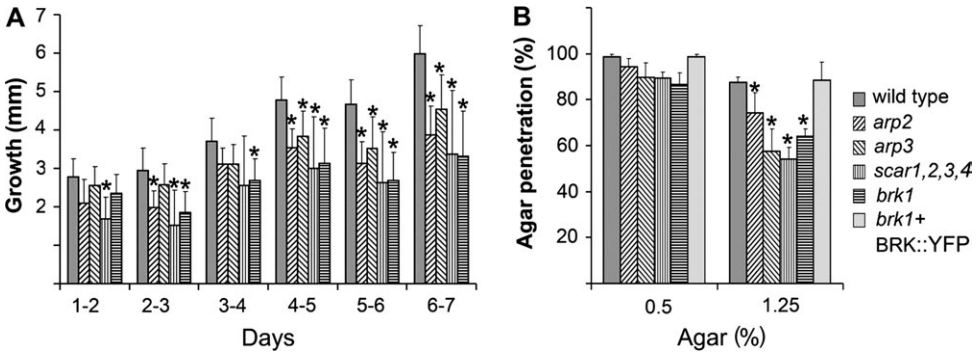

Figure 9. Growth Rate and Ability to Penetrate Agar Are Impaired in Roots of *arp2*, *arp3*, *scar1,2,3,4*, and *brk1* Mutants Compared to Wild-Type.

(A) Plants were grown on vertically oriented plates. Root lengths were measured daily for the same roots over a period of 1 week; daily increases in length are shown.

(B) Plants were grown on horizontally oriented plates containing growth medium supplemented with the indicated concentration of agar. The proportion of roots that penetrated the medium was scored after 7 d. Experiments were repeated two to four times, with at least 20 plants scored for each genotype. In A and B, error bars represent standard errors, and asterisks mark values that are significantly different from wild-type at the 99% confidence level.

typical junction in the wild-type consisted of a triangular-shaped pocket of middle lamella bordered by primary walls (arrow, Figure 10A). Abnormal junctions in *brk1* (arrow, Figure 10B) and *arp2* (arrow, Figure 10C) mutant roots were dramatically enlarged and filled with wall material having a distinct, abnormal texture (asterisks in Figure 10B and 10C).

Immunoelectron microscopy using a variety of antibodies described in Table 2 was employed to further compare wall composition in mutant and wild-type root tips. Anti-pectin antibodies JIM5 and JIM7 are widely used for immunolabeling of pectins, but showed very little labeling of either wild-type or mutant root tips (data not shown). Anti-pectin antibodies LM6 and CCRC-M38 (Table 2) gave stronger labeling signals and produced similar labeling patterns in wild-type and *brk1* mutant root tips (data not shown). Anti-pectin antibody CCRC-M22 and anti-xyloglucan antibody CCRC-M1 (Table 2) uniformly labeled the walls and intercellular junctions of wild-type root tip cells (Figure 10D and 10F). Consistent with the results of biochemical analyses showing no changes in the monosaccharide content of mutant root walls, the overall level and distribution of CCRC-M22 and CCRC-M1 labeling of walls and normal intercellular junctions were similar in *brk1* root tips compared to wild-type. In ultrastructurally abnormal intercellular junctions of *brk1* mutant root tips, CCRC-M22 and CCRC-M1 labeling was observed at the periphery but labeling with both antibodies was largely absent from the abnormal, internal areas (asterisks, Figure 10E and 10G). Thus, these junctions were filled with material of abnormal composition compared to normal cell corners.

DISCUSSION

While analysis of *Arabidopsis*, maize, and *Physcomitrella* mutants has established an important role for SCAR and ARP2/3 complexes in the regulation of plant cell growth, many questions have remained regarding the intracellular sites where these complexes function and the cellular processes dependent on this actin nucleation pathway. In this study, we focused on *Arabidopsis* SCAR1 and BRK1 proteins to address these questions. Several observations reported here support the conclusion that SCAR1 and BRK1, which bind directly to each other in vitro (Frank et al., 2004; Zhang et al., 2005), function together in vivo via a peripheral association with the plasma membrane. BRK1 and SCAR1 are both enriched in the membrane fraction and both behave biochemically as peripheral membrane proteins. BRK1 and SCAR1 are both localized to plasma membranes in several cell types and are similarly enriched at sites of active cell growth and wall deposition. BRK1 localization to the plasma membrane at cell corners is SCAR-dependent, supporting the conclusion that these proteins interact in vivo.

Plasma membrane localization of BRK1 and SCAR1 parallels earlier findings for animal cells where Scar and Arp2/3 complex subunits also localize to the plasma membrane (Machesky et al., 1997; Welch et al., 1997; Weiner et al., 1999; Miki et al., 1998; Nozumi et al., 2003; Stovold et al., 2005), but are perhaps surprising in relation to most previous work on plant SCAR and ARP2/3 complexes suggesting the cytoplasm as the primary location for the function of these complexes. In *Arabidopsis* SCAR and ARP2/3 complex subunit mutants, alterations in F-actin organization have been identified only in the cytoplasm of expanding trichomes. Immunolocalization of the Arp2/3 complex in the brown alga *Fucus* revealed polarized but primarily cytoplasmic localization of the complex in emerging rhizoids (Hable and Kropf, 2005). Immunostaining of elongating maize root hairs with antibodies raised against heterologous Arp3 proteins revealed cytoplasmic as well as tip-focused plasma membrane localization (Van Gestel et al., 2003). Furthermore, cytoplasmic localization was recently reported for *Arabidopsis* SCAR2 and BRK1 fluorescent fusion

Table 1. Chemical Composition of Cell Walls from Roots from 5-Day-Old Seedlings from Wild-Type (wt), *brk1*, and *arp2*.

	Neutral sugar composition (mol%)						
	Rha	Fuc	Ara	Xyl	Man	Gal	Glu
Wt	5.21 ± 0.14	3.42 ± 0.22	24.20 ± 1.47	15.18 ± 1.10	4.89 ± 0.57	37.43 ± 3.55	9.69 ± 0.59
brk1	4.84 ± 0.29	3.19 ± 0.27	25.16 ± 1.76	15.15 ± 1.34	4.33 ± 0.33	37.97 ± 4.3	9.35 ± 0.50
arp2	5.19 ± 0.28	3.47 ± 0.24	27.57 ± 1.47	15.85 ± 0.99	4.79 ± 0.39	33.16 ± 3.59	9.97 ± 0.42

Chloroform/methanol-insoluble material was used for sugar analysis. Measurements represent means ± standard errors (n = 4 for wt and *arp2*, n = 3 for *brk1*). [a] Rha, rhamnose; Fuc, fucose; Ara, arabinose; Xyl, xylose; Man, mannose; Gal, galactose; Glc, glucose.

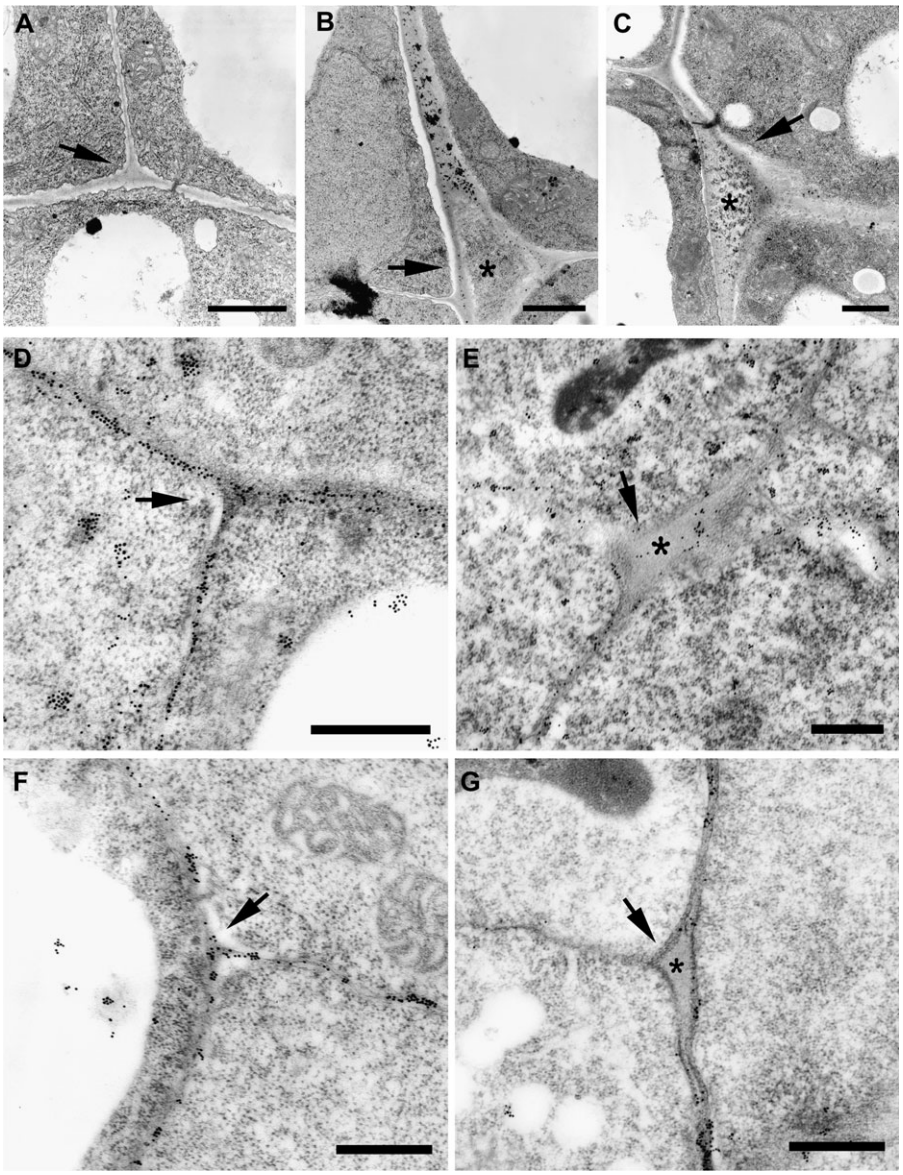

Figure 10. Cell Wall Ultrastructure and Composition Are Occasionally Altered at Three-Way Junctions in Root Tips of *brk1* and *arp2* Mutants.

(A–C) Cell wall ultrastructure visualized after osmium tetroxide post-fixation and uranyl acetate staining of wild-type (A), *brk1* mutant (B), and *arp2* mutant (C) root tips.

(D–G) Electron micrographs of wild-type (D, F) and *brk1* mutant (E, G) root tips labeled with CCRC-M1 anti-xyloglucan antibody (D, E) and CCRC-M22 anti-pectin antibody (F, G).

Arrows point to three-way wall junctions. Asterisks mark abnormally enlarged junctions seen only in mutant root tips, which are deficient in CCRC-M1 and CCRC-M22 labeling. Scale bar = 1 micron in (A–C); 0.5 micron in (D–G).

proteins transiently expressed in onion and *Arabidopsis* epidermal cells (Uhrig et al., 2007), but overexpression of these fusion proteins could account for the cytoplasmic localization in this case. Indeed, we also observed cytoplasmic localization of BRK1::YFP and GFP::SCAR1 when expressed from the 35S promoter in stable transformants, or transiently following bombardment into epidermal pavement cells (data not shown). Thus, we believe that expression of fusion proteins at low levels from their native promoters is needed to reveal the normal localization patterns of SCAR complex subunits.

Table 2. Antibodies Used for Characterization of Cell Walls.

Antibody	Antigens	Reference/source
CCRC-M1	Fucosylated xyloglucans	Freshour et al. (1996)
JIM5	HG	Clausen et al. (2003)
JIM7	HG	Clausen et al. (2003)
LM6	1→5-arabinan/RG-I	Willats et al. (1998)
CCRC-M22	De-arabinosylated RG-I	www.ccrc.uga.edu/~carbosource/CSS_home.html
CCRC-M38	Ubiquitous RG-I	www.ccrc.uga.edu/~carbosource/CSS_home.html

HG, homogalaturonan; RG, rhamnogalacturonan.

Our results demonstrating local concentration of SCAR complex subunits at sites of active cell growth and/or wall assembly are broadly consistent with the finding that ARP2/3 and SCAR complex subunits are localized at the growth site in elongating *P. patens* filaments. However, we found no detectable BRK1::YFP in tip-growing root hairs. Given the minor and largely redundant role played by the ARP2/3 complex in promoting root hair elongation in *Arabidopsis* (Mathur et al., 2003b; Deeks et al., 2007), we suggest that SCAR complex subunits are present in elongating root hairs at levels too low to detect. Alternatively, there may be a different ARP2/3 complex activator in root hairs, but this possibility is not supported by genetic studies nor are there any candidates for other ARP2/3 complex activator in plants. Thus, this possibility seems unlikely.

Our finding that SCAR1 and BRK1 associate peripherally with the plasma membrane in non-uniform patterns raises the question of how these proteins are localized. The ARP2/3 complex is thought to function downstream of the SCAR complex so would not be expected to participate in the localization of SCAR or BRK1. Indeed, in agreement with Perroud and Quatrano (2008), we found that the ARP2/3 complex is not required for BRK1 localization. We found that BRK1 localization depends on SCAR proteins, but the question remains as to how SCARs are localized. Recruitment of the Scar/WAVE complex to the plasma membrane in animal cells involves its interaction with the regulatory proteins Rac and Nck (Innocenti et al., 2004). The SRA1 subunit of the putative *Arabidopsis* SCAR complex binds to Rac-related proteins ROP2 and ROP4 (Basu et al., 2004), which are themselves plasma membrane-localized at growth sites of cells undergoing polarized expansion (Molendijk et al., 2001; Jones et al., 2002; Fu et al., 2002). More recently, it was shown that SPK1 is a positive regulator of ROP activity and associates with SCAR complex subunits in vivo (Basu et al., 2008). These findings suggest roles for SPK1 and ROPs in recruitment of the SCAR complex to appropriate sites on the plasma membrane, but this possibility remains to be tested.

Our localization results for SCAR complex subunits point to the plasma membrane as the primary site of SCAR and ARP2/3 complex-dependent actin polymerization in both leaves and roots. These results are consistent with our finding for maize *brk1* mutants that cortical F-actin enrichments associated with epidermal lobe outgrowth are completely lost (Frank and Smith, 2002; Frank et al., 2003). In *Arabidopsis*, however, we and others previously found no reduction of cortical F-actin density in abnormally expanding trichomes or pavement cells of SCAR and ARP2/3 complex subunit mutants, although a subtle alteration in the distribution of cortical actin was observed in pavement cells (e.g. Mathur et al., 2003a, 2003b; Le et al., 2003; Li et al., 2003; Basu et al., 2004; El-Assal et al., 2004; Djakovic et al., 2006). Loss of SCAR and ARP2/3 complex-dependent actin nucleation at the plasma membrane may cause changes in the dynamics of cortical F-actin that are important for proper regulation of trichome growth pattern but are too subtle to be observed by the methods used to date. Alternatively, abnormal trichome growth may result, as previously proposed (e.g. Mathur, 2006), from alterations to the cytoplasmic F-actin network, whose density and organization could depend directly or indirectly on actin nucleation at the plasma membrane. In contrast to the results for leaf epidermal cells, we did observe a marked reduction of cortical F-actin in internal tissue layers of *brk1* mutant root tips, demonstrating an important role for plasma membrane-localized SCAR complex subunits in accumulation of cortical F-actin in root cells.

Our results suggest that the SCAR–ARP2/3 actin nucleation pathway plays a role in cell wall assembly, consistent with a variety of earlier observations suggesting that actin functions in growing plant cells to direct the deposition of secreted wall components including pectins and xyloglucans (e.g. Foissner et al., 1996; Vissenberg et al., 2005; Chen et al., 2007). In particular, we observed that BRK1 and SCAR1 are enriched at cell corners, where locally increased deposition of cell wall material is presumably needed to fill the triangular-shaped spaces found at three-way wall junctions (e.g. Figure 10A, arrow). However, our analyses showed no clear differences in mutant root cell walls except for the occasional occurrence of three-way wall junctions with abnormal ultrastructure and composition (abnormally enlarged junctions containing material that is not labeled by anti-pectin or anti-xyloglucan antibodies). These abnormal junctions are a striking finding in relation to our observations that BRK1 and SCAR1 are enriched at cell corners adjacent to these junctions, and that cortical F-actin that normally accumulates preferentially at these corners is depleted in *brk1* mutants. Our observations suggest that the SCAR–ARP2/3 actin nucleation pathway participates in wall assembly at cell corners, and, by extrapolation, at other regions of the plasma membrane as well. As in root hair elongation

(Deeks et al., 2007), the role of the SCAR–ARP2/3 pathway in wall assembly may be largely redundant such that carbohydrate composition and ultrastructure are largely normal in SCAR and ARP2/3 complex mutants. However, more in-depth analyses of wall composition might reveal differences that could account for the reduced root rigidity we observed in SCAR and ARP2/3 complex mutants along with other previously described characteristics of these mutants such as their cell adhesion defects.

Taken together with results of earlier studies, our findings implicate SCAR and ARP2/3 complex-dependent actin polymerization in events occurring at the plasma membrane that promote normal cell growth and cell wall assembly. Regulation of membrane dynamics seems to be the most obvious possibility given the well established role played by the Arp2/3 complex in endocytosis in yeast and mammalian cells (Kaksonen et al., 2006; Sun et al., 2006; Merrifield et al., 2004, 2005). Endocytosis in plants is actin-dependent and has been proposed to be important for removal of excess membrane at sites of cell growth (e.g. Kang et al., 2003; Ovecka et al., 2005; Helling et al., 2006) as well as for wall assembly based on the observation of pectin in endosomes (Baluska et al., 2002; Dhonukshe et al., 2006). Thus, defects in endocytosis could explain many features of SCAR and ARP2/3 complex mutant phenotypes including reduced or aberrantly patterned cell growth in many tissues as well as the abnormal three-way wall junctions we observed in roots. Although the transient foci of Arp2/3 complex-dependent cortical F-actin associated with endocytosis in yeast and animal cells have not been observed in plant cells, this could be due to limitations of the imaging methods employed so far to visualize cortical F-actin in plant cells. An alternative (or additional) role for SCAR and ARP2/3 complex-dependent actin polymerization at the plasma membrane of plant cells could be to facilitate properly localized exocytosis. An exocytosis defect could also explain the variety of growth defects observed in mutants, and impairment in localized exocytosis of factors important for wall assembly could explain the abnormal three-way wall junctions we observed in *brk1* roots. Interestingly, a role for Arp2/3 complex-dependent actin polymerization in exocytosis has recently been suggested based on defects in myoblast fusion resulting from mutations in the Scar-related Arp2/3 complex activator WASP in *Drosophila* (Kim et al., 2007). Moreover, models envisioning a possible role for Arp2/3 complex-dependent actin polymerization in generating outward membrane curvature that could drive early events in exocytosis have also been recently proposed (Takenawa and Suetsugu, 2007). Further work will be needed to directly investigate possible roles for SCAR and ARP2/3 complex-dependent actin polymerization in endocytosis or exocytosis in plant cells.

METHODS

Plant Material

Mutants used in this study are described in Table 3. *scar1,2,3,4* quadruple mutants were constructed by crossing *scar1* to *scar2-DsLox* and the *scar3* and *scar4* mutations described in Table 3. *SCAR* genotypes were determined via PCR with gene-specific (G) and T-DNA or Ds-specific (I) primers listed in Table 4. The PIN1p::PIN1::GFP transgenic line (Heisler et al., 2005) was a gift from Jeff Long, Salk Institute. Plants used for phenotypic analysis were grown on MS medium without sucrose, solidified with 0.8% agar, unless otherwise indicated, and grown on a 16 h light/8 h dark cycle at 20–22°C.

Production Transgenic Plants Expressing Fluorescent Fusion Proteins

YFP and GFP fusion constructs were created using pEZRK-LNY and pEZS-CL, respectively, both gifts from David Ehrhardt,

Table 3. Mutants Used in this Study.

	Stock ID (source)	Genetic background	Mutation	RNA/protein levels	Reference
brk1	CS_86544 (ABRC)	Col (wild-type for ERECTA)	Early premature stop	Not tested	Djakovic et al., 2006; Le et al., 2006
arp2	SALK_077920 (ABRC)	Col	T-DNA insertion	No full-length mRNA by RT–PCR	Li et al., 2003
arp3	SALK_010045 (ABRC)	Col	T-DNA insertion	No full-length mRNA by RT–PCR	Li et al., 2003
scar1	FST line 123F07 (INRA–Versailles)	Ws	T-DNA insertion	Protein null	Djakovic et al., 2006
itb1-16/ scar2	David Oppenheimer, Univ. Florida	RLD	529-bp deletion	Not tested	Zhang et al., 2005
scar2-DsLox	Wisc–DsLox423A4 (ABRC)	Col	Modified Ds insertion	No full-length mRNA by RT–PCR (data not shown)	This study
scar3	SALK_036994	Col	T-DNA insertion	No full-length mRNA by RT–PCR	Zhang et al., 2008
scar4	GK_605G03 (GABI–Kat)	Col	T-DNA insertion	No full-length mRNA by RT–PCR (data not shown)	This study

Table 4. Primers Used for Genotyping *SCAR* Alleles.

Allele		Primer name	Sequence
scar1	G	34150–01	5′ CACGAATTCCCCATCTGATCATTCCTCCGGAA 3′
(FLAG/		34150–02	5′ GACCTCGAGAGATACCCTCTTCGGTTTCTCTCC 3′
FST	I	PFlag–LB	5′ CTACAAATTGCCTTTTCTTATCGAC 3′
123F07		34150–02	Above
scar2	G	38440–04F	5′ GGCAATGATGGAAGAAAGGTGG 3′
(Wisc		38440–04R6	5′ AATGCTCTCACCAGGAGATTTGG 3′
DsLox	I	38440–04F	Above
423A4		LB–DsLox	5′ AACGTCCGCAATGTGTTATTAAGTTGTC 3′
scar3	G	036994–F1	5′ GTTCACTCCAGGAAGACATTTGC 3′
(SALK_		036994–R2	5′ GTAGGAATTCTGCTCTGTTTCTTGC 3′
036994)	I	SALK–TDNA	5′ CCGTCTCACTGGTGAAAAGAA 3′
		036994–R2	Above
scar4	G	At01730GABI–GSF	5′ CTGAATTCCATGTGAAACTGAAGA 3′
(GK_		GK126B09-GSR	5′ TTTCTTGCCTTTGGTTCTGTATCT 3′
605G03)	I	At1730GABI–GSF	Above
		GABI–Kat T–DNA	5′ CCCATTTGGACGTGAATGTAGACAC 3′

For each indicated allele, the wild-type allele was identified with the G primer pair and the mutant allele with the I primer pair.

Carnegie Institution Dept of Plant Biology. To construct the SCAR2p::GFP::SCAR1 fusion, 0.8 kb of sequence upstream of the *SCAR2* (At2g38440) coding region was amplified from Columbia genomic DNA with primers 5′-GAGCTCTGAA-TAGATAATCTTGTTGCGT-3′ and 5′-GAATTCTGTTTGAGCTTCTC-TGTCTG-3′, and cloned into pEZRK-LNY in place of the CaMV 35S promoter. A full-length *SCAR1* (At2g34150) cDNA (Frank et al., 2004) was cloned downstream of GFP in pEZS-CL. A GFP::SCAR1fragment from this construct was then cloned into pEZRK-LNY downstream of the SCAR2 promoter in place of the YFP. The BRK1p::BRK1::YFP construct was created by amplifying the *BRK1* coding region (At2g22640) plus 1.26 kb of upstream sequence from Columbia genomic DNA with primers 5′-GCGGAGCTCATGTCGGAGAGCAAACCAAAG-3′ and 5′-CCG-GTACCGTCGCAAACAGAGAAGGATT-3′, and cloning an error-free PCR product upstream of YFP in pEZRK-LNY. BRK1p::BRK1::YFP was introduced into Columbia wild-type and *brk1* mutants, SCAR2p::GFP::SCAR1 was introduced into Columbia wild-type and *itb1-16/scar2* mutants and 35Sp::GFP::ABD2::GFP (Wang et al., 2008; a gift from Elison Blancaflor, The Noble Foundation) was introduced into Columbia wild-type and *brk1* mutants via *Agrobacterium*-mediated transformation using the floral dip method (Clough and Bent, 1998).

Transient Expression of BRK1::YFP

Eight-day-old seedlings were bombarded with 1-micron gold particles (Bio-Rad) coated with 20 ng BRK1p::BRK1::YFP plasmid using a Bio-Rad PDS-1000 helium biolistic system according to the manufacturer's instructions at a helium pressure of 1100 psi. Forty-eight hours later, leaf primordia were excised and imaged for BRK1::YFP fluorescence by confocal microscopy as described below.

Confocal Microscopy

BRK1::YFP, GFP::SCAR1, PIN1::GFP, and FM4-64 were imaged using spinning disk confocal microscope system equivalent to that described by Paredez et al. (2006), employing previously described methodology (Walker et al., 2007). Images were acquired and Z-stack projections assembled with MetaMorph software (Universal Imaging). GFP::ABD2::GFP was visualized using a Perkin Elmer UltraView ERS spinning disk confocal microscope using Perkin-Elmer ERS Ultra software. Z-stack projections were assembled and cross-sections were generated using Volocity 3.70 software (Improvision, Lexington, MA). For quantitative analysis of GFP::ABD2::GFP, the rectangular selection marquee tool of Volocity was used to measure average pixel intensities in selected areas, and intensity ratios were calculated as described in the text.

Root Growth Assays

To assay gravitropic responses, seedlings were grown vertically for 3 d in light on MS-agar plates and then rotated 90° and grown for another 24 h in darkness. Plates were scanned using an HP2510 scanner and root angles measured using ImageJ software version 1.36b (http://rsb.info.nih.gov/ij/). To assay root growth rates, seedlings were grown vertically on MS-agar plates. Daily increments of growth were determined by marking the position of the root tip on the back of the plate at 24-h intervals. To assay agar penetration of roots, seedlings were grown horizontally on MS plates containing 0.5 or 1.25% agar. At 7 d, roots were scored as having

penetrated the agar if they had made contact with the bottom of the plate.

BFA Treatment

Three-day-old PIN1p::PIN1::GFP and BRK1p::BRK1::YFP seedlings grown on MS agar-plates were transferred onto Whatman filter paper soaked with either 50 micromolar BFA (Sigma-Aldrich, St Louis, MO) in 0.28% DMSO or with DMSO only as a control. After 30 min, the seedlings were mounted onto slides and the fluorescent fusion proteins were imaged via confocal microscopy as described above.

Plasmolysis

Three-day-old seedlings expressing BRK1p::BRK1::YFP were mounted in water on slides and examined for YFP fluorescence via confocal microscopy as described above. Water was then carefully substituted by 5 micrograms ml^{-1} FM4-64 (Molecular Probes/Invitrogen, Carlsbad, CA) in 0.5 M sucrose, and roots were immediately imaged again for YFP and FM4-64 fluorescence.

Whole Mount Immunofluorescence

Actin immunolocalization in roots of 4-day-old seedlings was carried out as described by Rahman et al. (2007) with minor modifications (fixation was for 1 h in 50 mM PIPES, pH 7.2, with 20 mM EGTA and 20 mM $MgSO_4$ containing 2% paraformaldehyde, 0.1% Triton X-100 and 400 mm Maleimidobenzoyl-N-hydroxysuccinimide ester (Pierce/ThermoFisher Scientific, Rockford, IL), and wall digestion was for 20 min in 0.05% Pectolyase Y-23). To localize SCAR1, we used the protocol of Sugimoto et al. (2000), except that the fixative contained 2% formaldehyde and no glutaraldehyde, and sodium borohydride treatment was eliminated. Affinity-purified chicken anti-SCAR1 (Djakovic et al., 2006) was used at 5 micrograms ml^{-1} and Genway Biotech (San Diego, CA) FITC-anti-chicken IgY at 1:200. Samples were mounted in Vectashield (Vector Laboratories, Burlingame, CA) and root tips imaged using a Leica TCS SP2 AOBS confocal laser scanning microscope as described previously (Wang et al., 2008).

Transmission Electron Microscopy

Ultrastructural analysis was carried out as described by Meloche et al. (2007) except that seedlings were fixed initially for 1 h on agar plates by addition of 3% glutaraldehyde/0.05 M PIPES buffer (pH 7.4) directly to the plate and then in scintillation vials with fresh fixative solution (same as above) for another hour. For immunocytochemistry, tissue was embedded in LR White and processed as described by Meloche et al. (2007). A minimum of four grids were examined for each antibody treatment.

Microsome Preparation and Analysis of Membrane Association

Approximately 0.5 g of 14-day-old seedlings were homogenized in 1 ml TBS with 1 mM DTT, 10% sucrose and 1/100 plant protease inhibitor cocktail (Sigma) using an Omni TH homogenizer on ice. Supernantants following centrifugation at 16 000 *g* for 10 min were then centrifuged at 150 000 *g* for 40 min at 4°C to obtain a microsomal fraction. Analysis of conditions required for extraction of SCAR1 and BRK1::YFP from the microsomal was carried out as described by Boonsirichai et al. (2003). Briefly, the microsomal fractions were resuspended in the buffer described above supplemented with 2 M NaCl, 0.1 M Na_2CO_3, or 3% Triton X-100, incubated for 40 min at room temperature and centrifuged at 200 000 *g* for 60 min at 4°C. Supernatants were concentrated by precipitation using trichloroacetic acid.

Western Blot Analyses

Gel electrophoresis and Western blotting with anti-SCAR1 were carried out as previously described (Djakovic et al., 2006). For detection of BRK1::YFP, mouse anti-GFP (Zymed/Invitrogen, Carlsbad, CA) was used at 0.05 micrograms ml^{-1} followed by alkaline phosphatase-conjugated goat anti-mouse IgG (Promega, Madison, WI) diluted 1:10 000. Anti-α-1,2-Mannosidase I (Preuss et al., 2004) and anti-PUX1 (Rancour et al., 2004) were used to detect membrane and cytoplasmic proteins, respectively. Both antibodies were a gift from David Rancour, University of Wisconsin.

Analysis of Wall Composition

Neutral monosaccharides were measured by gas chromatography using a modification of the method of Blakeney et al. (1983), as follows. Roots were excised from 5-day-old seedlings and extracted in 10–12 changes of 1:1 chloroform:methanol over 4 d. The roots were pulverized using a ball mill and inositol was added as an internal standard to approximately 400 mg of the resulting residue. Roots were hydrolyzed in 2 M trifluoracetic acid in an autoclave for 1 h, and the resulting monosaccharides were derivatized to their alditol acetates, which were separated and measured using a Agilent 6890N gas chromatograph equipped with a Supelco SP2330 capillary column (30 m × 0.25 mm, 0.2 micron film thickness).

FUNDING

This work was supported by NSF grant IOB–0544226 to L.G.S.

ACKNOWLEDGMENTS

Thanks to members of the Smith laboratory for helpful discussions and comments on the manuscript, to James Ingham and Michael Burke for help with construction of *scar 1,2,3,4* quadruple mutants, to Elison Blancaflor for invaluable input and support of this work, and to ABRC and GABI-Kat for mutants. No conflict of interest declared.

REFERENCES

Baluska, F., Hlavacka, A., Samaj, J., Palme, K., Robinson, D.G., Matoh, T., McCurdy, D.W., Menzel, D., and Volkmann, D.

(2002). F-actin-dependent endocytosis of cell wall pectins in meristematic root cells: insights from brefeldin A-induced compartments. Plant Physiol. **130,** 422–431.

Basu, D., El-Assal Sel, D., Le, J., Mallery, E.L., and Szymanski, D.B. (2004). Interchangeable functions of *Arabidopsis* PIROGI and the human WAVE complex subunit SRA1 during leaf epidermal development. Development. **131,** 4345–4355.

Basu, D., Le, J., El-Assal Sel, D., Huang, C., Zhang, C., Mallery, E.L., Koliantz, G., Staiger, C.J., and Szymanski, D.B. (2005). DISTORTED3/SCAR2 is a putative Arabidopsis WAVE complex subunit that activates the Arp2/3 complex and is required for epidermal morphogenesis. Plant Cell. **17,** 502–524.

Basu, D., Le, J., Zakharova, T., Mallery, E.L., and Szymanski, D.B. (2008). A SPIKE1 signaling complex controls actin-dependent cell morphogenesis through the heteromeric WAVE and ARP2/3 complexes. Proc. Natl Acad. Sci. U S A. **105,** 4044–4049.

Blakeney, A.B., Harris, P.J., Henry, R.J., and Stone, B.A. (1983). A simple and rapid preparation of alditol acetates for monosaccharide analysis. Carbohydrate Res. **113,** 291–299.

Blancaflor, E.B., Wang, Y.S., and Motes, C.M. (2006). Organization and function of the actin cytoskeleton in developing root cells. Int. Rev. Cytol. **252,** 219–264.

Boonsirichai, K., Sedbrook, J.C., Chen, R., Gilroy, S., and Masson, P.H. (2003). ALTERED RESPONSE TO GRAVITY is a peripheral membrane protein that modulates gravity-induced cytoplasmic alkanilization and lateral auxin transport in plant statocytes. Plant Cell. **15,** 2612–2625.

Brembu, T., Winge, P., Seem, M., and Bones, A.M. (2004). *NAPP* and *PIRP* encode subunits of a putative WAVE regulatory protein complex involved in plant cell morphogenesis. Plant Cell. **16,** 2335–2349.

Chen, T., Teng, N., Wu, X., Wang, Y., Tang, W., Samaj, J., Baluska, F., and Lin, J. (2007). Disruption of actin filaments by Latrunculin B affects cell wall construction in *Picea meyeri* pollen tube by disturbing vesicle trafficking. Plant Cell Physiol. **48,** 19–30.

Clausen, M.H., Willats, W.G.T., and Knox, J.P. (2003). Synthetic methyl hexagalacturonate hapten inhibitors of anti-homogalacturonan monoclonal antibodies LM7, JIM5 and JIM7. Carbohydr. Res. **338,** 1797–1800.

Clough, S.J., and Bent, A.F. (1998). Floral dip: a simplified method for *Agrobacterium*-mediated transformation of *Arabidopsis thaliana*. Plant J. **16,** 735–743.

Deeks, M.J., Kaloriti, D., Davies, B., Malho, R., and Hussey, P.J. (2004). *Arabidopsis* NAP1 is essential for Arp2/3-dependent trichome morphogenesis. Curr. Biol. **14,** 1410–1414.

Deeks, M.J., Rodrigues, C., Dimmock, S., Ketelaar, T., Maciver, S.K., Malho, R., and Hussey, P.J. (2007). *Arabidopsis* CAP1: a key regulator of actin organisation and development. J. Cell Sci. **120,** 2609–2618.

Dhonukshe, P., Baluska, F., Schlicht, M., Hlavacka, A., Samaj, J., Friml, J., and Gadella, T.W., Jr (2006). Endocytosis of cell surface material mediates cell plate formation during plant cytokinesis. Dev. Cell. **10,** 137–150.

Djakovic, S., Dyachok, J., Burke, M., Frank, M., and Smith, L.G. (2006). ARP2/3 complex-dependent and -independent functions for BRICK1 in the spatial regulation of epidermal cell morphogenesis in *Arabidopsis*. Development. **133,** 1091–1100.

Eden, S., Rohtagi, R., Podtelejnikov, A.V., Mann, M., and Kirschner, M. (2002). Mechanism of regulation of WAVE1-induced actin nucleation by Rac1 and Nck. Nature. **418,** 790–793.

El-Assal, S.D., Le, J., Basu, D., Mallery, E.L., and Szymanski, D.B. (2004). *Arabidopsis GNARLED* encodes a NAP125 homolog that positively regulates ARP2/3. Curr. Biol. **14,** 1405–1409.

Finka, A., Schaefer, D.G., Saidi, Y., Goloubinoff, P., and Zyrd, J.P. (2007). In vivo visualization of F-actin structures during the development of the moss *Physcomitrella patens*. New Phytol. **174,** 63–76.

Foissner, I., Lichtscheidl, I.K., and Wasteneys, G.O. (1996). Actin-based vesicle dynamics and exocytosis during wound wall formation in Characean internodal cells. Cell Motil. Cytoskel. **35,** 35–48.

Frank, M., Egile, C., Dyachok, J., Djakovic, S., Nolasco, M., Li, R., and Smith, L.G. (2004). Activation of Arp2/3 complex-dependent actin polymerization by plant proteins distantly related to Scar/WAVE. Proc. Natl Acad. Sci. U S A. **101,** 16379–16384.

Frank, M.J., and Smith, L.G. (2002). A small, novel protein highly conserved in plants and animals promotes the polarized growth and division of maize leaf epidermal cells. Curr. Biol. **12,** 849–853.

Frank, M.J., Cartwright, H.N., and Smith, L.G. (2003). Three *brick* genes have distinct functions in a common pathway promoting polarized cell division and cell morphogenesis in the maize leaf epidermis. Development. **130,** 753–762.

Freshour, G., Clay, R.P., Fuller, M.S., Albersheim, P., Darvill, A.G., and Hahn, M.G. (1996). Development and tissue-specific structural alterations of cell wall polysaccharides of the Arabidopsis thaliana root. Plant Physiol. **110,** 1413–1429.

Fu, Y., Li, H., and Yang, Z. (2002). The ROP2 GTPase controls the formation of cortical fine F-actin and the early phase of directional cell expansion during *Arabidopsis* organogenesis. Plant Cell. **14,** 777–794.

Gautreau, A., Ho, H.Y., Steen, H., Gygi, S.P., and Kirschner, M.W. (2004). Purification and architecture of the ubiquitous WAVE complex. Proc. Natl Acad. Sci. U S A. **101,** 4379–4383.

Geldner, N., Friml, J., Stierhof, Y.D., Jurgens, G., and Palme, K. (2001). Auxin transport inhibitors block PIN1 cycling and vesicle trafficking. Nature. **413,** 425–428.

Goley, E.D., and Welch, M.D. (2006). The ARP2/3 complex: an actin nucleator comes of age. Nature Rev. Mol. Cell Biol. **7,** 713–726.

Hable, W.E., and Kropf, D.L. (2005). The Arp2/3 complex nucleates actin arrays during zygote polarity establishment and growth. Cell Motil. Cytoskeleton. **61,** 9–20.

Harries, P.A., Pan, A., and Quatrano, R.S. (2005). Arp2/3 complex component ARPC1 is required for proper cell morphogenesis and polarized cell growth in *Physcomitrella patens*. Plant Cell. **17,** 2327–2339.

Heisler, M.G., Ohno, C., Das, P., Sieber, P., Reddy, G.V., Long, J.A., and Meyerowitz, E.M. (2005). Patterns of auxin transport and gene expression during primordium development revealed by live imaging of the Arabidopsis inflorescence meristem. Curr. Biol. **15,** 1899–1911.

Helling, D., Possart, A., Cottier, S., Klahre, U., and Kost, B. (2006). Pollen tube tip growth depends on plasma membrane polarization mediated by tobacco PLC3 activity and endocytic membrane recycling. Plant Cell. **18,** 3519–3534.

Hussey, P.J., Ketelaar, T., and Deeks, M.J. (2006). Control of the actin cytoskeleton in plant cell growth. Annu. Rev. Plant Biol. **57,** 109–125.

Innocenti, M., et al. (2004). Abi1 is essential for the formation and activation of a WAVE2 signaling complex mediating Rac-dependent actin remodeling. Nature Cell Biol. **6,** 319–327.

Jones, M.A., Shen, J.-J., Fu, Y., Yang, Z., and Grierson, C.S. (2002). The *Arabidopsis* Rop2 GTPase is a positive regulator of both root hair initiation and tip growth. Plant Cell. **14,** 763–776.

Kaksonen, M., Toret, C.P., and Drubin, D.G. (2006). Harnessing actin dynamics for clathrin-mediated endocytosis. Nature Rev. Mol. Cell Biol. **7,** 404–414.

Kang, B.H., Busse, J.S., and Bednarek, S.Y. (2003). Members of the Arabidopsis dynamin-like gene family, ADL1, are essential for plant cytokinesis and polarized cell growth. Plant Cell. **15,** 899–913.

Kim, S., Shilagardi, K., Zhang, S., Hong, S.N., Sens, K.L., Bo, J., Gonzalez, G.A., and Chen, E.H. (2007). A critical function for the actin cytoskeleton in targeted exocytosis of prefusion vesicles during myoblast fusion. Dev. Cell. **12,** 571–586.

Kunda, P., Craig, G., Dominguez, V., and Baum, B. (2003). Abi, Sra1, and Kette control the stability and localization of Scar/WAVE to regulate the formation of actin-based protrusions. Curr. Biol. **13,** 1867–1875.

Le, J., El-Assal Sel, D., Basu, D., Saad, M.E., and Szymanski, D.B. (2003). Requirements for *Arabidopsis* ATARP2 and ATARP3 during epidermal development. Curr. Biol. **13,** 1341–1347.

Le, J., Mallery, E.L., Zhang, C., Brankle, S., and Szymanski, D.B. (2006). *Arabidopsis* BRICK1/HSPC300 is an essential WAVE-complex subunit that selectively stabilizes the Arp2/3 activator SCAR2. Curr Biol. **16,** 895–901.

Li, S., Blanchoin, L., Yang, Z., and Lord, E.M. (2003). The putative *Arabidopsis* Arp2/3 complex controls leaf cell morphogenesis. Plant Physiol. **132,** 2034–2044.

Machesky, L.M., Reeves, E., Wientjes, F., Mattheyse, F.J., Grogan, A., Totty, N.F., Burlingame, A.L., Hsuan, J.J., and Segal, A.W. (1997). Mammalian actin-related protein 2/3 complex localizes to regions of lamellipodial protrusion and is composed of evolutionarily conserved proteins. Biochem. J. **328,** 105–112.

Mathur, J. (2004). Cell shape development in plants. Trends Plant Sci. **12,** 583–590.

Mathur, J. (2006). Local interaction shape plant cells. Curr. Opin. Cell Biol. **18,** 40–46.

Mathur, J., Mathur, N., Kernebeck, B., and Hulskamp, M. (2003b). Mutations in actin-related proteins 2 and 3 affect cell shape development in *Arabidopsis*. Plant Cell. **15,** 1632–1645.

Mathur, J., Mathur, N., Kirik, V., Kernebeck, B., Srinivas, B.P., and Hulskamp, M. (2003a). *Arabidopsis CROOKED* encodes for the smallest subunit of the ARP2/3 complex and controls cell shape by region specific fine F-actin formation. Development. **130,** 3137–3146.

Meloche, C.G., Knox, J.P., and Vaughn, K.C. (2007). A cortical band of gelatinous fibers causes the coiling of redvine tendrils: a model based upon cytochemical and immunocytochemical studies. Planta. **225,** 485–498.

Merrifield, C.J., Perrais, D., and Zenisek, D. (2005). Coupling between clathrin-coated-pit invagination, cortactin recruitment, and membrane scission observed in live cells. Cell. **121,** 593–606.

Merrifield, C.J., Qualmann, B., Kessels, M.M., and Almers, W. (2004). Neural Wiskott–Aldrich syndrome protein (N-WASP) and the Arp2/3 complex are recruited to sites of clathrin-mediated endocytosis in cultured fibroblasts. Eur. J. Cell Biol. **83,** 13–18.

Miki, H., Suetsugu, S., and Takenawa, T. (1998). WAVE, a novel WASP-family protein involved in actin reorganization induced by Rac. EMBO J. **17,** 6932–6941.

Molendijk, A.J., Bischoff, F., Rajendrakumar, C.S.V., Friml, J., Braun, M., Gilroy, S., and Palme, K. (2001). Arabidopsis thaliana Rop GTPases are localized to tips of root hairs and control polar growth. EMBO J. **11,** 2779–2788.

Nozumi, M., Nakagawa, H., Miki, H., Takenawa, T., and Miyamoto, S. (2003). Differential localization of WAVE isoforms in filopodia and lamellipodia of the neuronal growth cone. J. Cell Sci. **116,** 239–246.

Ovecka, M., Lang, I., Baluska, F., Ismail, A., Illes, P., and Lichtscheidl, I.K. (2005). Endocytosis and vesicle trafficking during tip growth of root hairs. Protoplasma. **226,** 39–54.

Paredez, A.R., Somerville, C.R., and Ehrhardt, D.W. (2006). Visualization of cellulose synthase demonstrates functional association with microtubules. Science. **312,** 1491–1495.

Perroud, P.F., and Quatrano, R.S. (2006). The role of ARPC4 in tip growth and alignment of the polar axis in filaments of *Physcomitrella patens*. Cell Motil. Cytoskeleton. **63,** 162–171.

Perroud, P.F., and Quatrano, R.S. (2008). BRICK1 is required for apical cell growth in filaments of the moss *Physcomitrella patens* but not for gametophore morphology. Plant Cell. **20,** 411–422.

Preuss, M.L., Serna, J., Falbel, T.G., Bednarek, S.Y., and Nielsen, E. (2004). The *Arabidopsis* Rab GTPase RabA4b localizes to the tips of growing root hair cells. Plant Cell. **16,** 1589–1603.

Rahman, A., Bannigan, A., Sulaman, W., Pechter, P., Blancaflor, E.B., and Baskin, T.I. (2007). Auxin, actin, and growth of the *Arabidopsis thaliana* primary root. Plant J. **50,** 514–528.

Rancour, D.M., Park, S., Knight, S.D., and Bednarek, S.Y. (2004). Plant UBX domain-containing protein 1, PUX1, regulates the oligomeric structure and activity of *Arabidopsis* CDC48. J. Biol. Chem. **279,** 54264–54274.

Rogers, S.L., Wiedemann, U., Stuurman, N., and Vale, R.D. (2003). Molecular requirements for actin-based lamella formation in *Drosophila* S2 cells. J. Cell Biol. **162,** 1079–1088.

Royle, S.J., and Murrell-Lagnado, R.D. (2003). Constitutive cycling: a general mechanism to regulate cell surface proteins. Bioessays. **25,** 39–46.

Schwab, B., Mathur, J., Saedler, R., Schwarz, H., and Frey, B. (2003). Regulation of cell expansion by the *DISTORTED* genes in *Arabidopsis thaliana*: actin controls the spatial organization of microtubules. Mol. Genet. Genomics. **269,** 350–360.

Smith, L.G., and Oppenheimer, D.G. (2005). Spatial control of cell expansion by the plant cytoskeleton. Annu. Rev. Cell Dev. Biol. **21,** 271–295.

Stovold, C.F., Millard, T.H., and Machesky, L.M. (2005). Inclusion of Scar/WAVE3 in a similar complex to Scar/WAVE1 and 2. BMC Cell Biol. **6,** 11.

Stradal, T.E.B., and Scita, G. (2005). Protein complexes regulating Arp2/3-mediated actin assembly. Curr. Op. Cell Biol. **18,** 4–10.

Sugimoto, K., Williamson, R.E., and Wasteneys, G.O. (2000). New techniques enable comparative analysis of microtubule orientation, wall texture, and growth rate in intact roots of Arabidopsis. Plant Physiol. **124,** 1493–1506.

Sun, Y., Martin, A., and Drubin, D.G. (2006). Endocytic internalization in budding yeast requires coordinated actin nucleation and myosin motor activity. Dev. Cell. **11,** 33–46.

Szymanski, D.B. (2005). Breaking the WAVE complex: the point of *Arabidopsis* trichomes. Curr. Opin. Plant Biol. **8,** 103–112.

Takenawa, T., and Suetsugu, S. (2007). The WASP–WAVE protein network: connecting the membrane to the cytoskeleton. Nature Rev. Mol. Cell Biol. **8,** 37–48.

Uhrig, J.F., Mutondo, M., Zimmerman, I., Deeks, M., Machesky, L.M., Thomas, P., Uhrig, S., Hussey, P., and Hulskamp, M. (2007). The role of Arabidopsis genes in ARP2-ARP3-dependent cell morphogenesis. Development. **134,** 967–977.

Van Gestel, K., Slegers, H., Von Witsch, M., Samaj, J., Baluska, F., and Verbelen, J.P. (2003). Immunological evidence for the presence of plant homologues of the actin-related protein Arp3 in tobacco and maize: subcellular localization to actin-enriched pit fields and emerging root hairs. Protoplasma. **222,** 45–52.

Vissenberg, K., Fry, S.C., Pauly, M., Höfte, H., and Verbelen, J.-P. (2005). XTH acts at the microfibril–matrix interface during cell elongation. J. Exp. Bot. **56,** 673–683.

Walker, K.L., Müller, S., Moss, D., Ehrhardt, D.W., and Smith, L.G. (2007). *Arabidopsis* TANGLED identifies the division plane throughout mitosis and cytokinesis. Curr. Biol. **17,** 1827–1836.

Wang, Y.-S., Yoo, C.-M., and Blancaflor, E.B. (2008). Improved imaging of actin filaments in transgenic *Arabidopsis* plants expressing a green fluorescent protein fusion to the C- and N-termini of the fimbrin actin-binding domain 2. New Phytol. **177,** 525–536.

Weiner, O.D., Servant, G., Welch, M.D., Mitchison, T.J., Sedat, J.W., and Bourne, H.R. (1999). Spatial control of actin polymerization during neutrophil chemotaxis. Nature Cell Biol. **1,** 75–81.

Welch, M.D., DePace, A.H., Verma, S., Iwamatsu, A., and Mitchison, T.J. (1997). The human Arp2/3 complex is composed of evolutionarily conserved subunits and is localized to cellular regions of dynamic actin filament assembly. J. Cell Biol. **138,** 375–384.

Willats, W.G.T., Marcus, S.E., and Knox, J.P. (1998). Generation of a monoclonal antibody specific to (1→5) a-L-arabinan. Carbohydrate Res. **308,** 149–152.

Zhang, C., Mallery, E.L., Schlueter, J., Huang, S., Fan, Y., Brankle, S., Staiger, C.J., and Szymanski, D.B. (2008). *Arabidopsis* SCARs function interchangeably to meet actin-related protein 2/3 activation thresholds during morphogenesis. Plant Cell. **20,** 995–1011.

Zhang, X., Dyachok, J., Krishnakumar, S., Smith, L.G., and Oppenheimer, D.G. (2005). *IRREGULAR TRICHOME BRANCH1* in *Arabidopsis* encodes a plant homolog of the actin related protein2/3 complex activator Scar/WAVE that regulates actin and microtubule organization. Plant Cell. **17,** 2314–2326.